Journal of Power Sources 517 (2022) 230667

Contents lists available at ScienceDirect

Journal of Power Sources

journal homepage: www.elsevier.com/locate/jpowsour

An iterative analytical model for aging analysis of Li-ion cells

Mohammad Parhizi [a], Manan Pathak [b], Jason K. Ostanek [a,**], Ankur Jain [c,*]

[a] School of Engineering Technology, Purdue University, 401 N. Grant Street, West Lafayette, IN, 47907, USA
[b] BattGenie Inc., Seattle, WA, USA
[c] Mechanical and Aerospace Engineering Department, University of Texas at Arlington, 500 W First St, Rm 211, Arlington, TX, USA

HIGHLIGHTS

- Developed an iterative technique for aging analysis of Li-ion cells.
- Models capacity degradation due to cycling as well as calendar aging.
- Results shown to agree well with past work and numerical simulations.
- Results highlight key aspects of aging and capacity degradation in Li-ion cells.

ARTICLE INFO

Keywords:
Li-ion cell
Single particle model
SEI Formation
Green's function technique
Integral balance method

ABSTRACT

Physics-based aging models are critical for understanding capacity degradation mechanisms in Li-ion batteries. This paper presents a technique for aging analysis of a Li-ion cell due to growth of the solid electrolyte interphase (SEI) layer driven by a solvent decomposition reaction at the electrode surface. The model employs an iterative technique based on the analytical solutions of the underlying conservation equations. The single-particle model describing Li-ion intercalation and de-intercalation processes is solved analytically using Green's function technique. The SEI formation problem is solved using the integral balance method. An iterative technique that combines these analytical solutions is shown to result in a converged result within a few iterations. The model is shown to agree well with results from past studies, as well as a numerical simulation. The capacity fade of Li-ion batteries is investigated under different operating conditions and different regimes, including both cycling and storage. The present model offers much faster computation time than numerical models for modeling the degradation of Li-ion cells. Further, the iterative technique described here may serve as a framework for semi-analytical solutions for other, more complicated problems. This work contributes towards improving the performance and reliability of electrochemical energy conversion and storage systems.

1. Introduction

Li-ion batteries (LIBs) play a key role in energy conversion and storage in several engineering devices and systems, such as electric vehicles (EVs), renewable energy storage systems, and aerospace components [1,2]. While offering several advantages over other secondary batteries, capacity degradation and aging of Li-ion batteries does occur due to a variety of mechanisms [3]. An extensive amount of research has been carried out to understand the mechanisms underlying capacity loss in Li-ion batteries and predict the state of health of the cell. The formation and growth of a passive layer, called the Solid Electrolyte Interphase (SEI) layer, on the anode active material surface has often been considered the primary degradation mechanism in Li-ion batteries under typical battery usage conditions [3,4]. Typically, the reduction of electrolyte components such as ethylene carbonate (EC) through one or more side reactions is responsible for SEI growth [5]. SEI formation during initial cycling is critical for Li-ion batteries, since it blocks electron transfer and prevents further electrolyte decomposition. However, over a long time, continued SEI growth results in loss of active Lithium and, thus, capacity fade [3].

Since the calendar time required for experimental analysis of degradation and aging in Li-ion cells under real-life usage conditions may exceed years of storage or thousands of cycles, mathematical models are critical for understanding and improving the performance of Li-ion batteries [3]. Aging models can be broadly categorized into

* Corresponding author.
** Corresponding author.
E-mail addresses: jostanek@purdue.edu (J.K. Ostanek), jaina@uta.edu (A. Jain).

https://doi.org/10.1016/j.jpowsour.2021.230667
Received 3 June 2021; Received in revised form 1 September 2021; Accepted 19 October 2021

Nomenclature

A	electrode total interfacial surface area (m^2)
c_{EC}	solvent concentration within the SEI layer (mol m^{-3})
$c_{0,EC}$	initial solvent concentration within the SEI layer (mol m^{-3})
c_{eq}	solvent concentration in the bulk electrolyte (mol m^{-3})
c_{Li}	lithium concentration within the electrode particle (mol m^{-3})
c_{Li}^{max}	maximum lithium concentration within the electrode particle (mol m^{-3})
C	nominal capacity (Ah)
D_{EC}	solvent diffusion coefficient within the SEI layer ($m^2 s^{-1}$)
D_{Li}	lithium diffusion coefficient within the electrode particle ($m^2 s^{-1}$)
F	Faraday constant (96485 C mol^{-1})
I	applied current (A)
i	current density (Am^{-2})
J	molar flux (mol m^{-2} s^{-1})
k_{int}	rate constant of the intercalation reaction (m s^{-1})
$k_{f,s}$	rate constant of the side reaction (m s^{-1})
M_{SEI}	molecular weight of SEI (kg mol^{-1})
r	radial coordinate (m)
R	particle radius (m)
R_{SEI}	SEI resistance (Ω m^2)
R_u	universal gas constant (8.314 J mol^{-1} K^{-1})
t	time (s)
T	temperature (K)
U	open circuit potential (V)
V	total electrode volume (m^3)
β	cathodic charge transfer coefficient
δ_{SEI}	SEI layer thickness (m)
θ	lithium stoichiometry in the electrode
φ	potential (V)
κ_{SEI}	ionic conductivity (S m^{-1})
ρ_{SEI}	SEI density (kg m^{-3})
λ	eigenvalue (m^{-1})

Subscripts

0	initial
int	intercalation
n	anode
p	cathode
s	side reaction
surf	surface
t	total

empirical models, equivalent circuit or semi-empirical models, and electrochemical models [6]. Empirical models are data-driven and employ predictive algorithms such as artificial neural network (ANN) [7], Relevance Vector Machine (RVM) [8], and support vector machine (SVM) [9] to predict capacity fade based on past experimental data. Empirical models may require a substantial statistical population, and may not provide sufficient insights into the underlying physical phenomena. Equivalent circuit (EC) aging models are semi-empirical in nature with a certain degree of physicochemical support [6]. EC models employ electrical circuit components to simulate battery behavior. Electrochemical models on the other hand, are constructed based on the conservation equations that govern transport processes inside the battery. The most commonly used electrochemical model is the Pseudo-two-dimensional (P2D) model proposed by Doyle et al. [10]. P2D models have been used extensively for concentration, potential, state of charge (SoC), and state of health (SoH) prediction [11,12]. P2D models solve for concentration and potential gradient in both solid and liquid phases. The concentration within the solid phase is governed by the Fick's law of diffusion, while the concentration of Li-ions within the liquid-phase is governed by mass conservation [12].

While offering excellent accuracy, P2D models are computationally expensive due to the non-linear and coupled nature of the equations involved. Specifically, P2D models are not particularly suitable for modeling aging over thousands of cycles or several years of storage. Thus, a large number of previous studies has been devoted to reducing the complexity of electrochemical aging models [13,14]. A commonly used simplified version of the P2D model is the Single Particle (SP) model [15]. P2D models are reduced to SP models by neglecting concentration and potential gradients in the solution phase. Also, the pore wall flux at the electrode surface is usually assumed to be uniform throughout the electrode. Under these assumptions, the entire electrode can be represented by a single spherical particle, within which, diffusion can be described using Fick's second law. These assumptions are only valid for low to moderate charge/discharge rates or thin electrodes where the dynamics in the solution phase can be neglected. Despite its limitations, SP models have been shown to be well-suited with acceptable accuracy for aging analysis [3].

Although SP-based aging models are much simpler than full P2D models, existence of the side reactions results in coupled equations describing intercalation and SEI formation phenomena. The reason for this coupling is that while the total current density in the negative electrode is known, the individual intercalation and side reaction current densities are not known. These processes are difficult to model analytically, and therefore, only a few analytical studies of SEI formation are available, with various approximations, such as neglecting side reaction kinetics. For example, Ploehn et al. [16] developed an analytical solution for solvent diffusion through the SEI layer, followed by a two-electron reduction process at the carbon-SEI interface that results in SEI growth and capacity loss [16]. The analytical solution [16] resulted in a $\sqrt{t}$ evolution of the SEI thickness, similar to that in silicon oxidation [17] or Stefan-type phase change problems [18]. However, their model does not consider the kinetics of the side reaction. Pinson et al. [19] derived an analytical expression for the SEI growth based on a SP model. However, similar to the study by Ploehn et al. [16], the kinetics of the side reaction is neglected. Furthermore, linear solvent diffusion was assumed within the SEI layer [19]. Several numerical methods have been used to solve the SP-based aging models in previous studies. For example, Ramadass et al. [20] presented an aging model due to SEI growth during charge and discharge cycling. Solvent diffusion within the SEI layer was neglected in their work [20]. Ramasamy et al. [21] developed a capacity-fade model under open-circuit voltage (OCV) storage. The concentration of the solvent was considered to be constant at the electrode/SEI interface, and thus, the solvent diffusion within the SEI layer was neglected. Safari et al. developed a SP-based aging model for Li-ion batteries under different modes of operation for both kinetic and diffusion limited regimes [5]. Pang et al. developed an enhanced SP-based degradation model by considering SEI layer formation at the negative electrode [22]. Most of these models outlined above have been solved numerically. Numerical models require discretization in both the active material and the SEI film, resulting in large computational time and large memory required for calculation, which may not be suitable for field implementation. Therefore, a method capable of combining an analytical framework capable of capturing the underlying physics with efficient numerical computation is of much interest. Such a method can potentially offer good computational speed without loss of accuracy or stability problems, all within reasonable computational memory.

This paper presents a semi-analytical SP-based aging model for Li-ion batteries. Intercalation and SEI formation problems are first uncoupled

by initially assuming and then iteratively refining the side reaction current density as a function of time. The iterative refinement is based on analytical solution of the underlying conservation equations. Specifically, the intercalation problem is solved analytically using Green's function technique, and the SEI formation problem is solved using the integral balance method. Both sub-problems have closed-form solutions, which eliminates the need for discretization. Iteratively solving the two sub-problems is shown to result in convergence within a few iterations, with even a single iteration being sufficient for engineering accuracy in certain scenarios. The model is validated against a purely numerical computation and previous studies. The model is then used to determine the capacity fade of Li-ion batteries under different operating conditions and different regimes, including both cycling and storage. A key advantage of the present model is the elimination of the need for space discretization within the electrode particle and the SEI layer, which results in reduced computational time compared to numerical methods. Results from this work may help improve the understanding of degradation of Li-ion cells, and contribute towards improved electrochemical energy conversion and storage devices and systems.

2. Mathematical modeling

2.1. Problem definition and governing equations

Fig. 1(a) shows a schematic of a spherical anode particle operating under galvanostatic current density. The total current density in the negative electrode, i.e., $i_{t,n}$, is divided between the intercalation ($i_{int,n}$) and the side reaction (i_s) current densities, shown in Fig. 1(b). During charge and discharge processes, lithiated graphite undergoes a surface reaction with electrolyte solution species. This continuous small-scale reaction results in SEI formation, shown in Fig. 1(b). SEI growth results in an increase in electrode impedance and, consequently, an overall capacity loss. This section develops a novel semi-analytical aging model for Li-ion batteries to determine capacity loss rate under kinetic and diffusion-limited regimes. Kinetic-limited and diffusion-limited regimes are two ends of the spectrum of the aging mechanism. Depending on the conditions, the SEI growth within the cell may occur under either kinetic-limited, diffusion-limited, or somewhere in between. Whether the SEI growth is under kinetic- or diffusion-limited regime depends on a number of factors including cell chemistry, solvent diffusion coefficient within the SEI layer, diffusion coefficient of Li ions within the electrode particle, and the physical properties of the SEI product. In the kinetic-limited regime, solvent diffusion within the SEI layer is neglected i.e., the solvent is considered to be abundant at the anode/SEI interface and the side reaction is the rate-limiting process. In diffusion-limited regime, on the other hand, solvent diffusion within the SEI layer is the rate-limiting process.

A few assumptions are made prior to model development. First, SEI layer formation is considered to be the primary side reaction responsible for the aging of Li-ion cells [5]. Further, similar to previous studies [5, 23], the main component of the SEI layer is considered to be lithium ethylene dicarbonate $(CH_2OCO_2Li)_2$, radical anion formation ($EC + e^-_{graphite} \rightarrow EC^-$) is considered to be the rate-determining process. SEI is assumed to exist in single phase, and SEI growth on the anode particle is assumed to be uniform. Moreover, the cell and the SEI parameters are assumed to be independent of concentrations and temperature. Based on these assumptions, current balance for the graphite anode may be written as follows:

$$i_{t,n} = i_{int,n}(t) + i_s(t) \tag{1}$$

Note that for constant rate charge/discharge, the total current density is constant, whereas current densities associated with intercalation/deintercalation reactions and side reaction may change with time and are governed by the following Butler-Volmer kinetic expressions [24]:

$$i_{int,n}(t) = Fk_{int,n}c_{Li,n}^{\beta}\left(c_{Li,n}^{max} - c_{Li,n,surf}\right)^{1-\beta}\left[\exp\left(\frac{(1-\beta)F}{R_uT}\left(\varphi_{1n} - U_n - R_{SEI}i_{t,n}\right)\right) - \exp\left(-\frac{\beta F}{R_uT}\left(\varphi_{1n} - U_n - R_{SEI}i_{t,n}\right)\right)\right] \tag{2}$$

$$i_s(t) = -Fk_{f,s}c_{EC}|_{x=0}\exp\left(-\frac{\beta_s F}{R_uT}\left(\varphi_{1n} - R_{SEI}i_{t,n}\right)\right) \tag{3}$$

Where $R_{SEI} = \frac{\delta_{SEI}}{\kappa_{SEI}}$. All variables in equations (2) and (3) are defined in the nomenclature section. Note that equations (1)–(3) are written for the negative electrode. In case of the positive electrode, i_s and $R_{SEI}.i_{t,n}$ terms may be set to zero. The concentration of lithium inside the electrode particle is governed by Fick's diffusion law and may be written as follows:

$$\frac{\partial c_{Li,j}}{\partial t} = D_{Li,j}\frac{1}{r^2}\frac{\partial}{\partial r}\left(r^2\frac{\partial c_{Li,j}}{\partial r}\right) \tag{4}$$

where $j = n,p$ for the negative and positive electrode, respectively. The initial and boundary conditions are

$$c_{Li,j}(r, t=0) = c_{Li,0,j} \tag{5}$$

$$c_{Li,j}(r \rightarrow 0, t) \Rightarrow finite \tag{6}$$

$$\left(\frac{\partial c_{Li,j}}{\partial r}\right)_{r=R_j} = -\frac{i_{int,j}}{FD_{Li,j}} \tag{7}$$

Equation (5) models uniform initial concentration throughout the electrode particle. Equation (6) represents the boundary condition at the center of the electrode particle, requiring finiteness at the center. Equation (7) represents the boundary condition at the surface of the electrode that relates the intercalation current density to the lithium flux density. Material balance in the SEI film can be written as [5]:

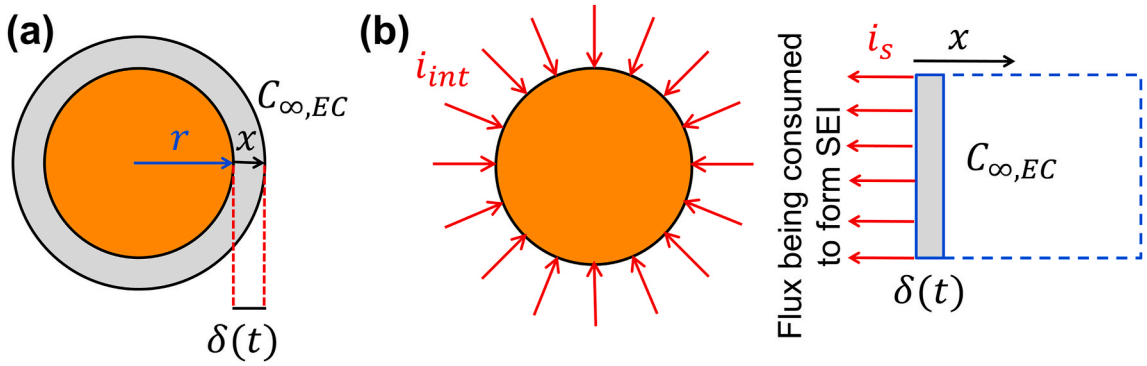

Fig. 1. Schematic of the problem showing (a) a spherical anode particle and growth of the SEI layer on its surface, (b) the uncoupled intercalation and SEI growth problems.

$$\frac{\partial c_{EC}}{\partial t} = D_{EC}\frac{\partial^2 c_{EC}}{\partial x^2} - \frac{d\delta_{SEI}}{dt}\frac{\partial c_{EC}}{\partial x} \tag{8}$$

Note that the first and second terms on the right-hand side of equation (8) represent mass transfer due to diffusion and convection, respectively. Since the thickness of the SEI layer is much smaller than the electrode particle, the SEI layer may be assumed to have a planar geometry [5]. As shown in Fig. 1(a), the origin for the Cartesian coordinate x is located at the electrode-SEI interface, i.e., at $r = R$. With reference to the Cartesian coordinate system, the initial and boundary conditions for the SEI layer growth process are:

$$c_{EC}(x, t=0) = c_{0,EC} \tag{9}$$

$$-D_{EC}\left(\frac{\partial c_{EC}}{\partial x}\right)_{x=0} + \frac{d\delta_{SEI}}{dt}(c_{EC})_{x=0} = \frac{i_s}{F} \tag{10}$$

$$c_{EC}(x = \delta_{SEI}, t) = c_{eq} \tag{11}$$

Equation (9) models uniform initial concentration throughout the initial SEI thickness. Equation (10) relates the side reaction current density to the lithium flux density due to diffusion and convection. Furthermore, equation (11) represents an equilibrium EC concentration at the electrolyte/SEI interface assuming the electrolyte composition does not change. Finally, the rate of SEI growth can be determined from the side reaction current density as follows [5]:

$$\frac{d\delta_{SEI}}{dt} = -\frac{i_s M_{SEI}}{2F\rho_{SEI}} \tag{12}$$

Governing equations for the solid-phase diffusion (equations (4)–(7)) and material balance within the SEI layer (equations (8)–(12)) are closely coupled to each other since the intercalation/deintercalation current density, $i_{int,n}$, and side reaction current density, i_s, are both unknown and related to each other through equation (1). In general, solving these equations simultaneously is challenging both theoretically and numerically. The next section describes an iterative, semi-analytical technique for solving these equations.

2.2. Iterative semi-analytical technique

This study presents an iterative technique to uncouple solid-phase diffusion and material balance in the SEI layer. This technique has been used previously to solve problems related to heat transfer in three-dimensional integrated circuits 3D ICs [25], conjugate phase change heat transfer [26,27], and single-phase conjugate heat transfer [28]. However, it does not appear to have been used to solve concentration diffusion problems, such as the one in this work. In this technique, the problem of interest is divided into two sub-problems, each with available analytical solutions individually. Specific to the present work, the solid-phase diffusion problem is solved analytically using Green's function approach - capable of accounting for time-dependent current density - developed in a recent study [29] and material balance in the SEI layer is solved using an approximate analytical technique due to the non-linear nature of the equations involved.

Starting with an assumed/guessed boundary condition for both sub-problems, the analytical solutions are used iteratively to improve upon the guess based on the results, and repeat until the solution is converged. The algorithm for the iterative approach is shown in Fig. 2. Note that in each step, the variables shown in green are known, while the variables in red are unknown and need to be calculated. The procedure starts with an initial guess for the side reaction current density, i_s, as a function of time. Based on this, the intercalation/deintercalation current density, $i_{int,n}(t)$, and SEI thickness, $\delta_{SEI}(t)$, are determined from equations (1) and (12), respectively. With this information, the solid phase diffusion sub-problem is solved analytically using Green's function approach described in the following subsection. Once the lithium concentration at the electrode's surface is known, the cell potential, φ_n, is calculated using the Butler-Volmer kinetics represented by equation (2). Next, the concentration of EC at the SEI-electrode interface is determined by solving equations (8)–(11) using the integral method described in the following sub-sections. Finally, the side reaction current density, i_s, is re-calculated using equation (3) and compared with the initial guess. If the comparison lies within the desired tolerance, the solution is considered to be converged; otherwise, the newly calculated i_s is used as the refined guess, and iteration is continued until the convergence is achieved. Since deriving a rigorous mathematical proof to establish convergence of the iterative technique is likely to be extremely challenging, mainly because of the complexity and non-linearity of the underlying equations, the convergence of the method is established numerically by investigating multiple cases with initial guesses varying in nature and magnitude.

While this is an iterative technique, subsequent sections in this paper

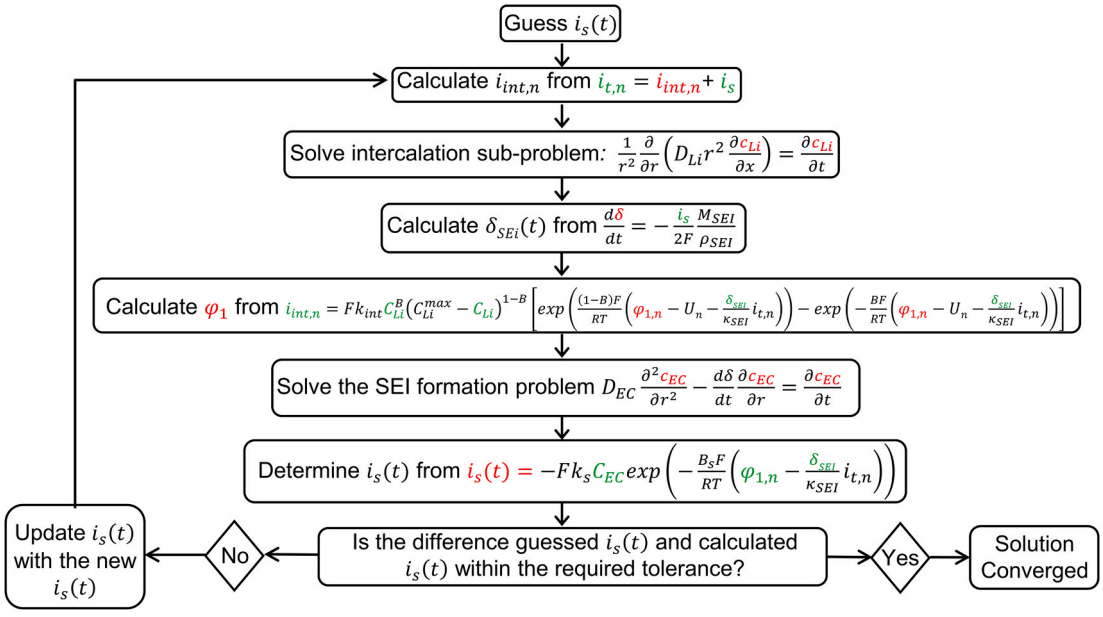

Fig. 2. Flowchart of the iterative algorithm used in this study. Parameters shown in green and red are known in advance and to be computed, respectively. (For interpretation of the references to colour in this figure legend, the reader is referred to the Web version of this article.)

show that the solution converges very rapidly within a few iterations. In certain cases, even a single iteration is sufficient. Further, the converged solution is found to be insensitive to the initial guess. A key advantage of this technique is that the species concentration needs to be calculated only at the electrode-SEI interface for both Li and EC, which eliminates the computational burden associated with having nodes within the electrode and the SEI layer.

The iterative approach described above requires solutions for two sub-problems i.e., solid phase diffusion and SEI formation. These solutions are presented in the next sub-sections.

2.3. Analytical solution of solid phase diffusion

Green's function based analytical solution of lithium concentration profile within the electrode particle operating under a time-dependent current density was presented in a recent paper [29]. Assuming low current densities and/or thin electrodes, concentration gradient and potential in the solution phase is neglected. Under these assumptions, the concentration at the surface of the positive and negative electrode particles can be written as follows [29]:

$$c_{Li,j,surf}(t) = c_{Li,0,j} - \frac{3}{R_j}\int_{\tau=0}^{t} J_j(\tau)d\tau - \sum_{m=1}^{\infty}\frac{1}{N_{m,j}}\sin^2\left(\lambda_{m,j}R_j\right) \int_{\tau=0}^{t} J_j(\tau)\exp\Big(-D_{Li,j}\lambda_{m,j}^2(t-\tau)\Big)d\tau \tag{13}$$

where the eigenvalues $\lambda_{m,j}$ are the positive roots of $R_jX_j\cot(R_jX_j) = 1$, and $j = n,p$ for the negative and positive electrode, respectively. $N_{m,j}$ is the norm, defined as:

$$N_{m,j} = \frac{R_j\left(\lambda_{m,j}^2 + \frac{1}{R_j^2}\right) - \frac{1}{R_j}}{2\left(\lambda_{m,j}^2 + \frac{1}{R_j^2}\right)} \tag{14}$$

The molar flux for the cathode and anode can be written as:

$$J_p(t) = \frac{I(t)}{A_pF} \tag{15}$$

$$J_n(t) = -\frac{(I(t) - i_sA_n)}{A_nF} \tag{16}$$

Note that the sign of the current, I, is considered to be negative for discharge and positive for charge. Details of the mathematical derivation of the surface concentration can be found in a recent paper [29].

2.4. Closed-form solution of SEI sub-problem

Integral method is used to solve the governing equations associated with the concentration of EC in the SEI layer presented in equations 8–12. The integral method has been used for the analysis of boundary layer momentum and energy equations in fluid mechanics [30], thermal convection [31], and phase change related moving boundary problems [32]. In this method, the relevant conservation equation (equation (8) in the present work) is integrated over the appropriate transport region, such as thermal/momentum boundary layer or SEI thickness, ($\delta_{SEI}(t)$ in the present work). The quantity of interest, such as temperature, velocity or concentration within the evolving layer is modeled as a polynomial function, with coefficients chosen to satisfy the various boundary conditions. Finally, the assumed concentration profile is substituted back in the integrated conservation equation, resulting in an ordinary differential equation (ODE) for the thickness of the layer of interest. Once the thickness is known, it is substituted back into the assumed profile to construct the distribution of the variable of interest, c_{EC} in this case.

Note that in the SEI sub-problem, the SEI layer thickness, $\delta_{SEI}(t)$ is known from equation (12), since the side reaction current density, $i_s(t)$ is guessed. Instead, the concentration of EC at the electrode surface $c_w(t)$ is not known. Thus, a small modification to the integral method is introduced, which results in an ODE for $c_w(t)$ instead of $\delta_{SEI}(t)$. To begin with, equation (8) is integrated using Leibniz's integral formula, resulting in:

$$D_{Li}\left(\frac{\partial c_{EC}}{\partial x}\bigg|_{x=\delta_{SEI}(t)} - \frac{\partial c_{EC}}{\partial x}\bigg|_{x=0}\right) - \frac{d\delta_{SEI}}{dt}\left(c_{EC}|_{x=\delta_{SEI}(t)} - c_{EC}|_{x=0}\right) = \frac{d}{dt}\left(\int_{x=0}^{\delta_{SEI}(t)} c_{EC}dx - \delta_{SEI}c_{EC}|_{x=\delta_{SEI}}\right) \tag{17}$$

Next, a third-degree polynomial is assumed for the concentration of EC in the SEI film as follows:

$$c_{EC}(x,t) = a + b(x - \delta_{SEI}(t)) + c(x - \delta_{SEI}(t))^2 + d(x - \delta_{SEI}(t))^3 \tag{18}$$

Four boundary conditions are required to determine coefficients a, b, c and d. Two boundary conditions are already defined by equations (10) and (11). The third boundary condition is constructed based on equation (11), i.e., $c_{EC}(x = \delta_{SEI}, t) = c_{eq}$, which implies that the total change in the concentration at δ_{SEI} is zero. Thus, differentiating equation (11) results in:

$$dc_{EC} = \left[\frac{\partial c_{EC}}{\partial x}dx + \frac{\partial c_{EC}}{\partial t}dt\right]_{x=\delta_{SEI}} = 0 \tag{19}$$

Equation (19) can be written as:

$$\left[\frac{\partial c_{EC}}{\partial x}\frac{d\delta_{SEI}}{dt} + \frac{\partial c_{EC}}{\partial t}\right]_{x=\delta_{SEI}} = 0 \tag{20}$$

Comparing equation (20) and equation (8) results in the following third boundary condition:

$$\left(D_{EC}\frac{\partial^2 c_{EC}}{\partial x^2}\right)_{x=\delta_{SEI}} = 0 \tag{21}$$

The last boundary condition is written on the basis of the concentration of EC at the electrode-SEI interface as follows:

$$c_{EC}(x = 0, t) = c_w(t) \tag{22}$$

$c_w(t)$ is not known in advance, and is determined as a function of δ_{SEI} from equation (17). Next, coefficients a, b, c and d are determined from four boundary conditions and the assumed temperature profile, equation (18) is substituted back into equation (17). After some mathematical manipulation, the following ODE is derived for $c_w(t)$:

$$\frac{dc_w}{dt} = \frac{1}{\left(5\delta + \frac{\delta'\delta^2}{D_{EC}}\right)}\left(12D_{EC}\left(\frac{c_{eq} - c_w(t)}{\delta}\right) - 3\delta'\left(c_{eq} + 3c_w(t) + \frac{8\rho}{M}\right) - \frac{(\delta^2\delta'' + 2\delta\delta'^2)\left(c_w(t) + \frac{2\rho}{M}\right)}{D_{EC}}\right) \tag{23}$$

Concentration of EC at the electrode-SEI interface, $c_w(t)$ appears in equation (3) for side reaction current density calculation. Thus, the ODE given by equation (23) is the only equation needed to be solved for the SEI sub-problem. The initial condition associated with equation (23) is given simply by equation (9).

3. Results and discussion

3.1. Convergence of the iterative technique

This sub-section discusses convergence of the iterative technique outlined in Section 2. All the parameters used in this study are obtained

Table 1
Li-ion cell parameters used for modeling [5]. The parameters are shown for the anode and cathode of a Sony 18650 Li-ion cell used for cycling and OCV storage, and for the anode of an MP prototype prismatic cell used for constant-potential storage.

Parameters	Sony 18650 Cell		SAFT MP Prototype (Half-Cell)
	Anode	Cathode	Anode
R (μm)	2.0	2.0	1.0
c_{Li}^{max} (mol m^{-3})	30555	51555	30555
A (m^2)	4.38	4.76	21.5
D_{Li} (m^2 s^{-1})	2×10^{-14}	1×10^{-14}	2×10^{-14}
k_{int} (m s^{-1})	2.07×10^{-11}	1.04×10^{-11}	1.04×10^{-11}
β	0.5	0.5	0.5
θ	0.74 (Cycling) 0.99 (OCV)	0.5 (Cycling)	0.9 (Constant Potential Storage)

Table 2
Solid electrolyte interface (SEI) parameters used in the present study [5].

Parameter	Value
$R_{SEI,0}$ (Ω m^2)	0.001
c_{eq} (mol m^{-3})	227.05
M_{SEI} (kg mol^{-1})	0.162
ρ_{SEI} (kg m^{-3})	1690
$\delta_{SEI,0}$ (nm)	5.0
κ_{SEI} (S m^{-1})	5×10^{-6}
β_s	0.5
D_{EC} (m^2 s^{-1})	6.8×10^{-21}(Cycling) 3.7×10^{-19}(OCV Storage)
$K_{f,s}$ (m s^{-1})	1.36×10^{-12}(Cycling) 1.36×10^{-7}(OCV Storage)

from previous study by Safari et al. [5] and summarized in Tables 1 and 2. The 18650 Sony cell parameters presented in Table 1 are used for these simulations. Fig. 3(a) and (b) plot the side reaction current density, i_s as a function of time under kinetic-limited and diffusion-limited regimes, respectively. In each case, sub-Figure (i) presents the plot for a single discharge prosses and sub-Figure (ii) presents the plot for a single charge process. A constant current is taken as the initial guess for these simulations, and shown as the 0th iteration in the plots. Fig. 3(a) shows that the i_s curve converges within two iterations under kinetic-limited regime, beyond which, the deviation between successive iterations is less than 0.1%. The computational time for each iteration is around 0.3 s. It is also seen that the side reaction current density for discharge processes under both regimes is extremely small, indicating minimal contribution of discharge process in SEI growth.

Fig. 3(b) shows that similar to the kinetic-limited regime, the side reaction current density converges within two iterations. For the charging process shown, however, the side reaction current density converges within six iterations. This could be explained by the difference between the equations governing kinetic-limited and diffusion-limited regimes. In the kinetic-limited scenario, the concentration of EC is constant; thus, the material balance equations are not needed to be solved, resulting in a much simpler problem than the diffusion-limited regime. Even with six iterations, however, the computational cost is minimal compared to a fully-numerical approach that may involve extensive discretization.

Since limited information is available for making the initial guess, it is important to determine whether the converged solution for iterative techniques is independent of the initial guess. In order to demonstrate that the method converges to the same curve independent of the magnitude of the initial guess, Supplementary Fig. S1 presents the converged side reaction current density as a function of time for initial guesses that are 3 and 5 orders of magnitude smaller and larger than the converged curve for both (a) kinetic- and (b) diffusion-limited regimes. It is shown that the side reaction current density converges to the same curve regardless of the magnitude of the initial guess. To investigate this further, the iterative technique is used for solving kinetic- and diffusion-controlled charge processes with three different initial guesses of the side reaction current – constant (Case A), linearly decreasing (Case B), and sinusoidally-varying (Case C). Fig. 4(a) shows convergence of side reaction current density as a function of time regardless of the nature of the initial guess under a kinetic-limited regime. Note that in Fig. 4(a), the initial guess is 5 orders of magnitude less than the converged

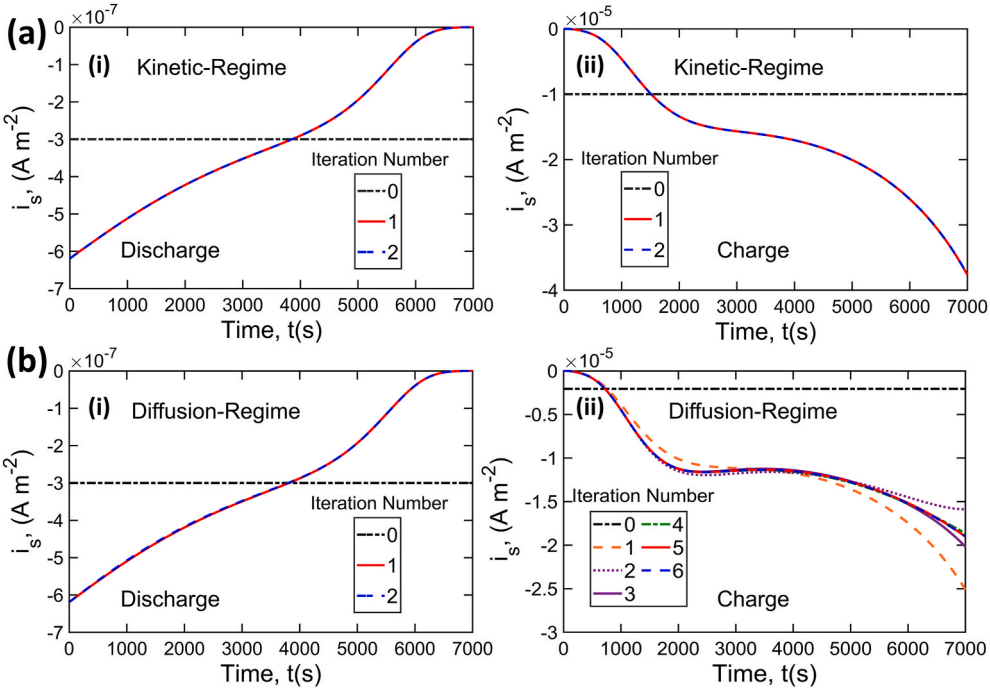

Fig. 3. Convergence of the iterative technique for cycling under (a) kinetic-limited regime and (b) diffusion-limited regime. In each case, plots are presented for side reaction current density as a function of time for (i) discharge process, and (ii) charge process.

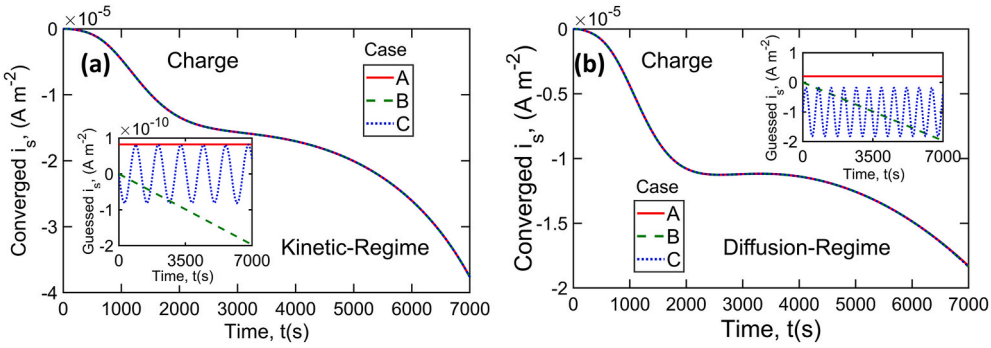

Fig. 4. Plots showing convergence of the iterative technique independent of the nature of initial guess under (a) kinetic-limited regime and (b) diffusion-limited regime: side reaction current density as a function of time for three different cases of a constant (A), linear (B), and periodic (C) initial guesses during a charge process for multiple initial guesses 5 orders of magnitude smaller and larger than the converged curves.

solution, indicating that prior knowledge of the initial guess and its magnitude is not required for convergence. In each case, convergence is obtained within two iterations. Such independence of the solution from the initial guess is important to establish because in general, there is limited basis for choosing an initial guess, and therefore, the technique must result in accurate converged solution regardless of the choice of the initial guess. Fig. 4(b) plots the converged side reaction current density as a function of time for different initial guess functions under a diffusion-limited regime. In this case, the initial guess is around 5 orders of magnitude larger than the converged solution. Similar to the kinetic-limited regime, the converged current density is independent of the initial guess. Nevertheless, the side reaction current density is usually only a very small fraction (less than 1%) of the total current density. Therefore, an estimate of 0.1% of total current is recommended as a reasonable and robust initial guess with which to initiate the iterative computational technique.

3.2. Model validation against numerical simulation

A comparison of the iterative technique with fully numerical

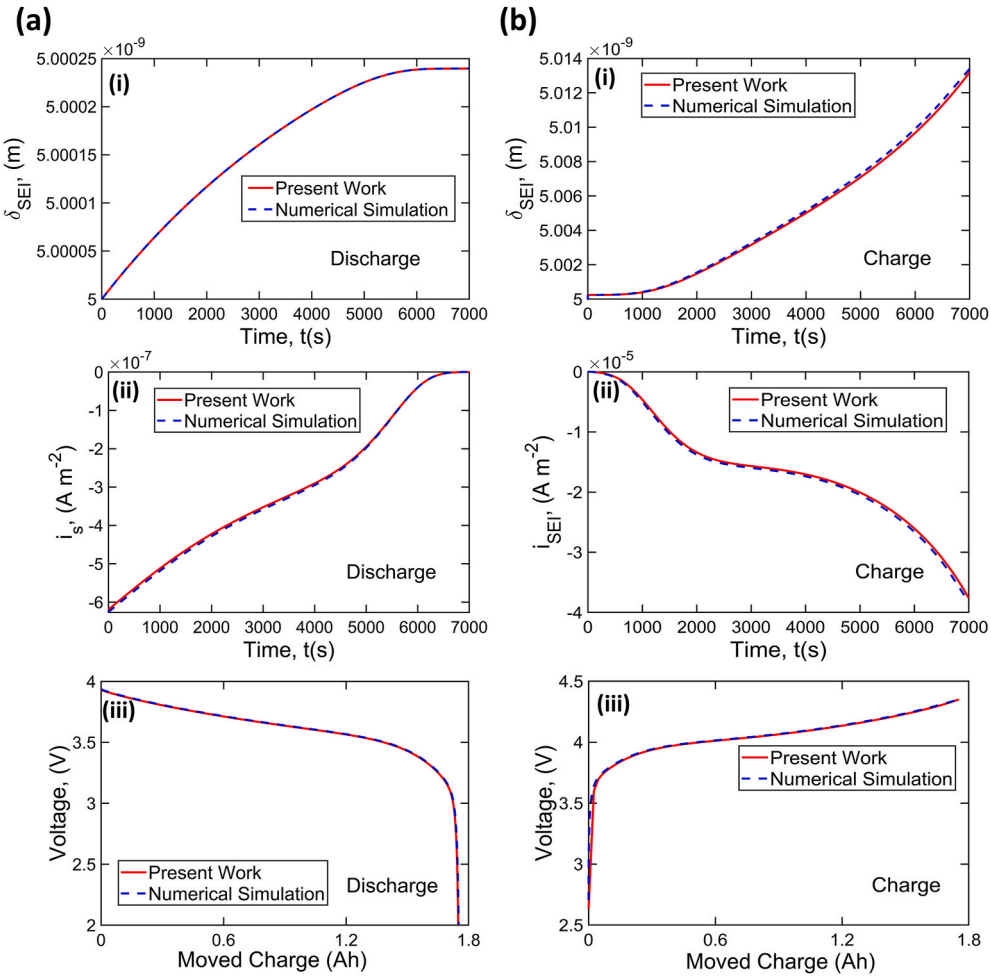

Fig. 5. Comparison of the present work with numerical simulation for the first cycle during a kinetically-limited (a) discharge and (b) charge processes. In each case, plots are presented for (i) SEI growth as a function of time, (ii) side reaction current density as a function of time, (iii) voltage as a function of moved charge.

simulation is presented next for both kinetic-limited and diffusion-limited regimes. The parameters used for comparison for both the kinetic and diffusion-limited are presented in Tables 1 and 2. Similar to the previous section, parameters for the 18650 Sony cell are used for these simulations. Numerical simulation is carried out by discretizing the governing equations using a finite difference method. The resulting set of nonlinear differential algebraic equations (DAEs) are solved using a robust index-1 DAE solver [33] technique in Maple 2020. Comparison plots for the first cycle under the kinetic-limited regime are shown in Fig. 5(a) and (b) during the discharge and charge process, respectively. In each case, plots are presented for (i) SEI thickness as a function of time, (ii) side reaction current density as a function of time, and (iii) voltage as a function of the moved charge. These figures show excellent agreement between the iterative technique and numerical simulations for each case, with a maximum error of less than 1%. Convergence is obtained within two iterations, with a minimal computation time of 0.6 s. It is seen that the side reaction current density is flat and equal to zero at the end of the discharge and beginning of the charge process where the SoC is low. This is expected due to the existence of the potential in the exponential term in equation (3). Consequently, the SEI growth follows a similar trend, being zero at the end of discharge and beginning of the charge process. Furthermore, a comparison between the charge and discharge process shows that the SEI growth due to the discharge process is negligible compared to the charge process.

A similar comparison for the diffusion-limited regime is shown in Fig. 6(a) and (b) during a discharge and charge process, respectively. For

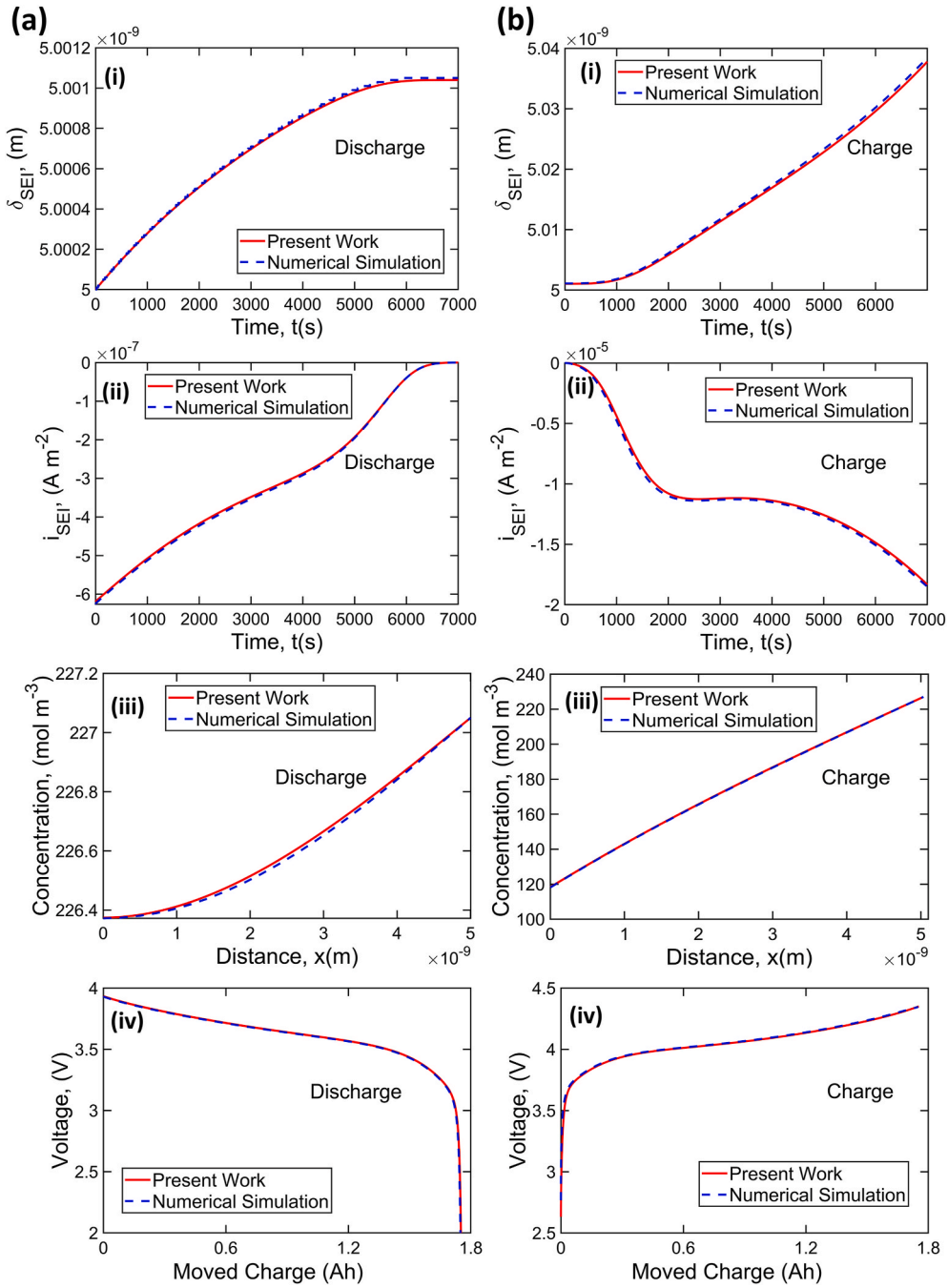

Fig. 6. Comparison of the present work with numerical simulation for the first cycle during a diffusion-limited (a) discharge and (b) charge process. In each case, plots are presented for (i) SEI growth as a function of time, (ii) side reaction current density as a function of time, (iii) solvent concentration distribution in the SEI at the end of the process, and (iv) voltage as a function of moved charge.

each case, plots of SEI thickness and sider eaction current density as functions of time are presented in (i) and (ii). The concentration of the solvent, c_{EC}, within the SEI layer is plotted as a function of SEI thickness in (iii). Finally, cell voltage as a function of moved charge during the discharge process for the first cycle is shown in (iv). Both sets of figures show excellent agreement with numerical simulation in predicting the cell electrochemical behavior during charging and discharging. The convergence is achieved within two and six iterations for the discharge and charge process, respectively. Similar to the kinetic-limited regime, contribution of discharge in SEI formation is minimal, resulting in a very small solvent concentration gradient within the SEI layer. However, during the charge process, the solvent concentration gradient within the SEI layer is significant.

3.3. Applications and model validation against past work

The iterative approach is now used to model multi-mode aging mechanisms. The three different aging mechanisms considered in this section are capacity fade during charge/discharge cycling, capacity fade during open-circuit voltage (OCV) storage, and capacity fade during constant voltage storage.

3.3.1. Aging during charge/discharge cycling

This subsection analyzes the capacity loss of an 18650 $LiCoO_2$ Li-ion cell during charge/discharge cycling under a constant current. The cell nominal capacity is 1.8 Ah, and different charge/discharge rate are considered. Similar to the previous work [5], two extreme scenarios of kinetic-limited and diffusion-limited SEI growth are considered here and shown in Fig. 7(a) and (b), respectively. The parameters used in this section are presented in Tables 1 and 2. For each case, (i) plots the SEI resistance, R_{SEI}, as a function of the number of cycles up to 800 cycles for 0.5C, (ii) plots the cell discharge voltage as a function of the moved charge for different cycle numbers for 0.5C, (iii) plots the normalized capacity of the cell as a function of the number of cycles. For the kinetic-limited regime (Fig. 7(a) (i) and (ii), results from a previous study by Safari et al. [5] are also shown. It is seen that the results from the present study are in excellent agreement with past work. It is also seen that SEI resistance increases linearly and consequently, the cell capacity decreases linearly during cycling for the kinetic-limited regime and the cell capacity decreases due to the SEI growth. Fig. 7(a)(iii) shows that the capacity loss increases as the C-rate decreases. This is consistent with results from previous studies [19,34]. Similar to these previous studies, capacity loss due to SEI layer formation has been formulated in the present work as the integral of side reaction current density with time, resulting in an increase in capacity fade with a decrease in the C-rate due to the increased charging/discharging time. In other words, lower C-rates provide more time for the side reaction to occur, while for high C-rates, the charge time is lower, and hence correspondingly, the total fade due to SEI is also lower [34]. Please note that the present study considers aging under low C-rates where SEI formation is the primary mechanism of aging. Other mechanisms that occur at high C-rates, such as overcharge and mechanical stress, are not considered here, and may increase degradation at large C-rates.

Fig. 7(b) present similar plots to Fig. 7(a), respectively, but for a

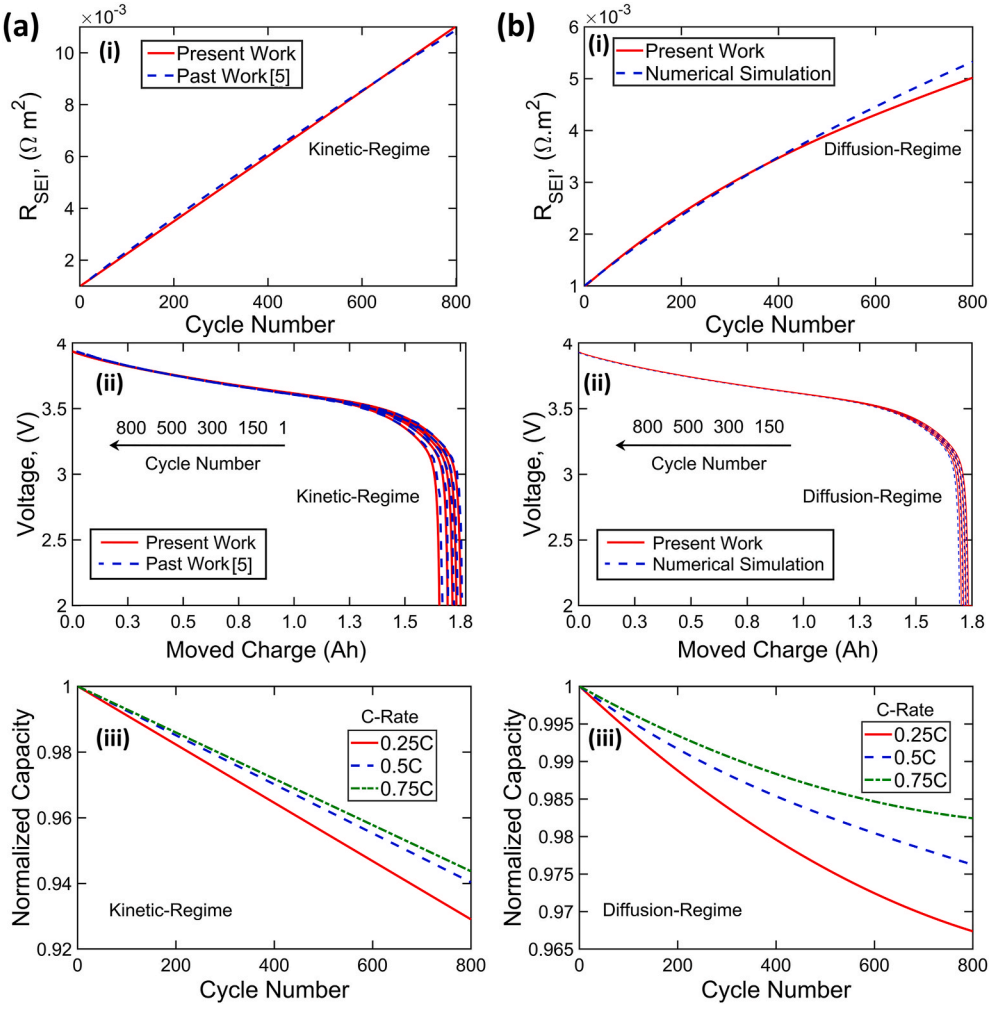

Fig. 7. Applications and comparison of the present model with previous studies and numerical simulations under cycling for (a) kinetically-limited and (b) diffusion-limited regimes. In both cases, plots are presented for (i) SEI resistance as a function of number of cycles for 0.5C, (ii) cell voltage as a function of moved charge at different cycle numbers for 0.5C, (iii) normalized cell capacity as a function of number of cycles for multiple C-rates. Results are compared with a past work [5], and with numerical simulations in (a) and (b), respectively.

diffusion-limited regime. It is seen that under diffusion-limited regime, the SEI resistance grows and cell capacity decreases quadratically compared to the linear growth under kinetic-limited regime during charge/discharge cycling. Results from the fully numerical simulation presented in section 3.2 are also shown in these figures for comparison. It is seen that the semi-analytical model is in good agreement with the numerical simulation. The SEI resistance determined from the iterative approach is identical to the numerical simulation up to 500s and slightly diverges from the numerical simulation at higher cycles with a maximum error of around 5%. A possible reason behind this small error is the approximation involved in assuming a polynomial form for concentration distribution within the SEI layer. The accuracy of the model may possibly be further improved by considering higher order polynomials, which, however, may require additional, appropriately developed boundary conditions. Experimental data are required to determine the appropriate regime for the SEI growth. Furthermore, similar to Fig. 7 (a)(iii), Fig. 7(b)(iii) shows that the capacity loss increases as the C-rate decreases due to the longer charge/discharge time at lower discharge rates.

3.3.2. Aging during OCV storage

This subsection analyzes the capacity loss during open-circuit potential storage. Li-ion cells are subject to a capacity loss and a voltage decrease under OCV storage. Under OCV storage, lithium ions de-intercalate from graphite and reacts at the surface of the particle to form SEI. Consequently, the SOC of the electrode decreases, resulting in anode potential rise. Ramasamy et al. [21] have reportedexperimental data for the anode potential rise of an 18650 Li-ion cell under OCV storage at 25 °C. Safari et al. [5] predicted anode potential rise under a diffusion-limited regime and their results were in good agreement with experimental data. A similar analysis is carried out using the semi-analytical model presented in this study. The cell and the side reaction parameters are summarized in Tables 1 and 2. Fig. 8 (a) shows the anode potential rise as a function of the number of days. Results from the numerical simulation by Safari et al. [5] and experimental data reported by Ramasamy et al. [21] are also shown in Fig. 8 (a). It is seen that the present work is in very good agreement with both past studies.

3.3.3. Aging during constant voltage storage

This sub-section investigates the aging of Li-ion cells due to storage under a constant potential. Broussely et al. [35] reported the capacity loss of a 5Ah prismatic MP prototype cell stored under a constant voltage of 3.9 V and a temperature of 30 °C. Safari et al. [5] presented a numerical physics-based aging model for the constant potential storage under kinetic-limited and diffusion-limited regimes. Their results indicated that the diffusion-limited regime was in better agreement with the experimental data from Broussely et al. [35]. The semi-analytical model presented here is used to model aging during constant potential storage. Similar to Safari et al. [5], a constant cell voltage of 3.9 V corresponding to an initial SOC of 90% is considered. Also, the analysis is carried out for the graphite half-cell only. The parameters for the graphite half-cell summarized in Tables 1 and 2 are used for modeling this aging mechanism. The side reaction parameters are assumed similar to those used for cycling except for the diffusion coefficient and the side reaction rate constant. Since the refined parameters for these two were not explicitly reported in Safari et al. [5], they were fitted in the present study. Fig. 8(b) plots the capacity loss as a function of the square root of the number of storage days. The capacity loss is calculated from $C_{Loss}(t) = \frac{\theta A_n \rho}{M C_0} \delta_{SEI}$, as suggested by Ploehn et al. [16]. It is seen that for both regimes, results are in very good agreement with past work by Safari et al. [5]. Also, it is seen that results from the diffusion-limited regime are in better agreement with past experimental data taken from Ploehn et al. [16].

3.4. Effect of the polynomial degree on the concentration profile

Equation (18) shows the third-degree polynomial form assumed for the variation of solvent concentration within the SEI layer. It may be possible to assume an even simpler polynomial form, such as quadratic or linear to further reduce computation time. The impact of the polynomial degree on the accuracy of the converged solution is investigated next by comparing results for linear and quadratic forms with the third-degree polynomial results. Two different values of the solvent diffusion coefficient are considered. Supplementary Figs. S2(a) and S2(b) show the solvent concentration profile at the end of a discharge and charge process, respectively. The same range of vertical access is chosen for both charge and discharge plots. The solvent diffusion coefficient is considered to be $D_{EC} = 6.8 \times 10^{-21}$ $m^2 s^{-1}$. Supplementary Fig. S2(a) shows that the polynomial degree does not affect the predicted concentration profile by much. The inset in Supplementary Fig. S2(a) shows the zoomed view of the concentration profile. Although the nature of the curves is different for the three profiles as shown in inset, the difference between the magnitudes is negligible. This occurs since the contribution of the discharge process in the SEI formation is negligible and often ignored in aging simulations. Supplementary Fig. S2(b), on the other hand, shows that the first-degree polynomial approximation results in a large error especially at the electrode-SEI interface. The second-degree and third-degree polynomials are shown to be closer to each other. Supplementary Figs. S3(a) and S3(b) present similar plots, but for an order of magnitude larger solvent diffusion coefficient. These plots show that the difference between the three profiles decreases as the diffusion coefficient increases, as expected. In fact, sufficiently large solvent diffusion coefficient may convert the diffusion-limited regime into the kinetic-limited regime, where diffusion within the SEI layer is ignored.

Note that, polynomial fitting technique used in this work is expected to provide reasonable accuracy, since the order of polynomial used for fitting is limited to third-order and no extrapolation is involved – the spatial range is always limited to $0<x<\delta_{SEI}$, at the ends of which, the polynomial fit is designed to obey boundary conditions.

3.5. Advantages of the present model

The iterative technique discussed in this work, offers a few key

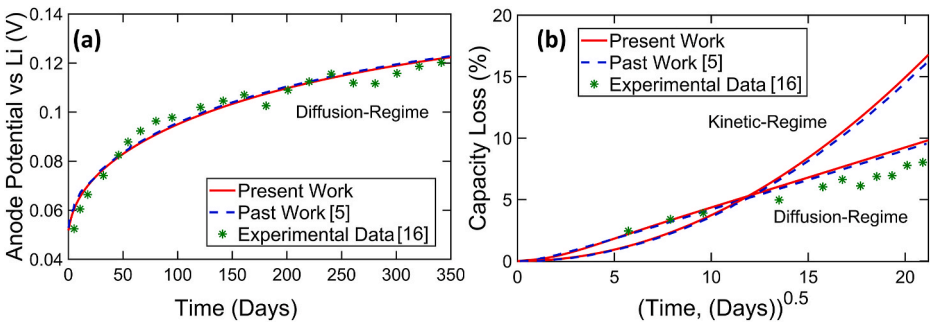

Fig. 8. Applications and comparison of the present model with previously reported experimental data: (a) anode potential rise as a function of number of days under OCV storage for an 18650 cell; (b) Capacity loss as a function of square root of number of days for kinetic- and diffusion-controlled regimes for a SAFT MP Prototype half-cell. Values of cell parameters for both are listed in Table 1. In both cases, results from the present work are presented along with past numerical [5] and experimental [16] studies.

advantages over numerical models and conventional iterative solvers used for SP-based aging modeling. Firstly, the iterative approach presented here is constructed from analytical, closed-form solutions of the governing equations. Consequently, full spatial discretization is avoided and the solution is needed to be calculated only at a single node. In comparison, other methods generate a large number of algebraic equations due to spatial discretization, which is much more computationally intensive. Moreover, numerical solvers may fail while trying to find consistent initial conditions for the algebraic variables using the initial conditions for the ODE variables, due to stiffness of the governing equations. Furthermore, the iteration is carried out on the entire time domain at once compared to some numerical approaches in which iteration for convergence is required at each timestep. The reduced computational time and memory needed by the iterative model described here may facilitate more effective parametric studies of the impact of various parameters on cell degradation, as well as optimized techniques for improving the reliability of practical energy conversion and storage systems.

4. Conclusions

An iterative semi-analytical approach is used in this work to model capacity loss and aging of Li-ion batteries under different operating conditions. The primary aging mechanism is considered to be the decomposition and reduction of the solvent resulting in the formation of the SEI layer. The intercalation of Li-ion within the electrode is accounted for using the SP model, and thus, solution phase concentration and potential gradient is neglected. Note that this assumption is only valid for low to moderate C-rates. The model is developed by uncoupling intercalation and the SEI-formation sub-problems. The uncoupling is carried out by initially assuming and then iteratively refining the side reaction current density as a function of time. The intercalation problem is solved analytically using Green's function technique, and the SEI formation problem is solved using the integral balance method. The model presented here eliminates the need for discretization, resulting in low computational costs. Results from this work may help develop better understanding of degradation of Li-ion cells, and eventually contribute towards improved electrochemical energy conversion and storage. Furthermore, the present work may be used as the baseline for developing semi-analytical models for more complicated problems such as the full P2D framework.

CRediT authorship contribution statement

Mohammad Parhizi: Conceptualization, Methodology, Formal analysis, Investigation, Validation, Data curation. **Manan Pathak:** Methodology, Investigation. **Jason K. Ostanek:** Methodology, Investigation, Supervision. **Ankur Jain:** Conceptualization, Methodology, Investigation, Data curation, Supervision, Project administration, All authors contributed towards Writing – original draft, Writing – review & editing.

Declaration of competing interest

The authors declare that they have no known competing financial interests or personal relationships that could have appeared to influence the work reported in this paper.

Acknowledgments

Mohammad Parhizi acknowledges the Purdue Polytechnic Institute Post-Doctoral Fellowship Program for financial support on this project. This material is partly based upon work supported by CAREER Award No. CBET-1554183 from the National Science Foundation.

Appendix A. Supplementary data

Supplementary data to this article can be found online at https://doi.org/10.1016/j.jpowsour.2021.230667.

References

[1] J.B. Goodenough, K.S. Park, The Li-ion rechargeable battery: a perspective, J. Am. Chem. Soc. 135 (4) (Jan 30 2013) 1167–1176, https://doi.org/10.1021/ja3091438.
[2] B. Scrosati, J. Garche, Lithium batteries: status, prospects and future, J. Power Sources 195 (9) (2010) 2419–2430, https://doi.org/10.1016/j.jpowsour.2009.11.048.
[3] C. Delacourt, M. Safari, Mathematical modeling of aging of Li-ion batteries, in: A. Franco, M. Doublet, W. Bessler (Eds.), Physical Multiscale Modeling and Numerical Simulation of Electrochemical Devices for Energy Conversion and Storage, Springer, 2016, pp. 151–190.
[4] A.J. Smith, J.C. Burns, X. Zhao, D. Xiong, J.R. Dahn, A high precision coulometry study of the SEI growth in Li/graphite cells, J. Electrochem. Soc. 158 (5) (2011), https://doi.org/10.1149/1.3557892.
[5] M. Safari, M. Morcrette, A. Teyssot, C. Delacourt, Multimodal physics-based aging model for life prediction of Li-ion batteries, J. Electrochem. Soc. 156 (3) (2009), https://doi.org/10.1149/1.3043429.
[6] M. Lucu, E. Martinez-Laserna, I. Gandiaga, H. Camblong, A critical review on self-adaptive Li-ion battery ageing models, J. Power Sources 401 (2018) 85–101, https://doi.org/10.1016/j.jpowsour.2018.08.064.
[7] R.G. Jungst, et al., Accelerated calendar and pulse life analysis of lithium-ion cells, J. Power Sources 119–121 (2003) 870–873, https://doi.org/10.1016/s0378-7753(03)00193-9.
[8] D. Wang, Q. Miao, M. Pecht, Prognostics of lithium-ion batteries based on relevance vectors and a conditional three-parameter capacity degradation model, J. Power Sources 239 (2013) 253–264, https://doi.org/10.1016/j.jpowsour.2013.03.129.
[9] A. Nuhic, T. Terzimehic, T. Soczka-Guth, M. Buchholz, K. Dietmayer, Health diagnosis and remaining useful life prognostics of lithium-ion batteries using data-driven methods, J. Power Sources 239 (2013) 680–688, https://doi.org/10.1016/j.jpowsour.2012.11.146.
[10] M. Doyle, T.F. Fuller, J. Newman, Modeling of galvanostatic charge and discharge of the lithium/polymer/insertion cell, J. Electrochem. Soc. 140 (6) (1993) 1526–1533, https://doi.org/10.1149/1.2221597.
[11] A. Tulsyan, Y. Tsai, R.B. Gopaluni, R.D. Braatz, State-of-charge estimation in lithium-ion batteries: a particle filter approach, J. Power Sources 331 (2016) 208–223, https://doi.org/10.1016/j.jpowsour.2016.08.113.
[12] A. Jokar, B. Rajabloo, M. Désilets, M. Lacroix, Review of simplified Pseudo-two-Dimensional models of lithium-ion batteries, J. Power Sources 327 (2016) 44–55, https://doi.org/10.1016/j.jpowsour.2016.07.036.
[13] V. Ramadesigan, V. Boovaragavan, J.C. Pirkle, V.R. Subramanian, Efficient reformulation of solid-phase diffusion in physics-based lithium-ion battery models, J. Electrochem. Soc. 157 (7) (2010), https://doi.org/10.1149/1.3425622.
[14] V.R. Subramanian, V. Boovaragavan, V. Ramadesigan, M. Arabandi, Mathematical model reformulation for lithium-ion battery simulations: galvanostatic boundary conditions, J. Electrochem. Soc. 156 (4) (2009), https://doi.org/10.1149/1.3065083.
[15] S. Atlung, K. West, T. Jacobsen, Dynamic aspects of solid solution cathodes for electrochemical power sources, J. Electrochem. Soc. 126 (8) (1979) 1311–1321, https://doi.org/10.1149/1.2129269.
[16] H.J. Ploehn, P. Ramadass, R.E. White, Solvent diffusion model for aging of lithium-ion battery cells, J. Electrochem. Soc. 151 (3) (2004), https://doi.org/10.1149/1.1644601.
[17] J.C. Slattery, Advanced Transport Phenomena, Cambridge University Press, 1999.
[18] D.W. Hahn, M.N. Özışık, Heat Conduction, third ed., Wiley, Hoboken, N.J., 2012, p. 1, online resource (746 p.).
[19] M.B. Pinson, M.Z. Bazant, Theory of SEI formation in rechargeable batteries: capacity fade, accelerated aging and lifetime prediction, J. Electrochem. Soc. 160 (2) (2013) A243–A250, https://doi.org/10.1149/2.044302jes.
[20] P. Ramadass, B. Haran, P.M. Gomadam, R. White, B.N. Popov, Development of first principles capacity fade model for Li-ion cells, J. Electrochem. Soc. 151 (2) (2004), https://doi.org/10.1149/1.1634273.
[21] R.P. Ramasamy, J.-W. Lee, B.N. Popov, Simulation of capacity loss in carbon electrode for lithium-ion cells during storage, J. Power Sources 166 (1) (2007) 266–272, https://doi.org/10.1016/j.jpowsour.2006.12.086.
[22] H. Pang, L. Mou, L. Guo, F. Zhang, Parameter identification and systematic validation of an enhanced single-particle model with aging degradation physics for Li-ion batteries, Electrochim. Acta 307 (2019) 474–487, https://doi.org/10.1016/j.electacta.2019.03.199.
[23] X. Lin, J. Park, L. Liu, Y. Lee, A.M. Sastry, W. Lu, A comprehensive capacity fade model and analysis for Li-ion batteries, J. Electrochem. Soc. 160 (10) (2013) A1701–A1710, https://doi.org/10.1149/2.040310jes.
[24] A.J. Bard, L.R. Faulkner, Electrochemical Methods : Fundamentals and Applications, second ed., xxi, Wiley, New York, 2001, p. 833.
[25] L. Choobineh, A. Jain, Analytical solution for steady-state and transient temperature fields in vertically stacked 3-D integrated circuits, IEEE Trans. Compon. Packag. Manuf. Technol. 2 (12) (2012) 2031–2039, https://doi.org/10.1109/tcpmt.2012.2213820.

[26] M. Parhizi, A. Jain, Analytical modeling and optimization of phase change thermal management of a Li-ion battery pack, Appl. Therm. Eng. 148 (2019) 229–237, https://doi.org/10.1016/j.applthermaleng.2018.11.017.
[27] M. Parhizi, A. Jain, Theoretical modeling of a phase change heat transfer problem with a pre-melted or pre-solidified region, Int. J. Heat Mass Tran. 136 (2019) 635–643, https://doi.org/10.1016/j.ijheatmasstransfer.2019.02.079.
[28] K. Shah, A. Jain, An iterative, analytical method for solving conjugate heat transfer problems, Int. J. Heat Mass Tran. 90 (2015) 1232–1240, https://doi.org/10.1016/j.ijheatmasstransfer.2015.07.056.
[29] M. Parhizi, A. Jain, Analytical modeling of solid phase diffusion in single-layer and composite electrodes under time-dependent flux boundary condition, J. Electrochem. Soc. 167 (6) (2020), https://doi.org/10.1149/1945-7111/ab847c.
[30] H. Schlichting and K. Gersten, Boundary-Layer Theory, ninth ed., pp. 1 online resource (XXVIII, 805 p. 288 illus.).
[31] A. Mostafavi and A. Jain, "Unsteady convective heat transfer from a flat plate with heat flux that varies in space and time," Int. J. Heat Mass Tran., vol. 172, 2021, doi: 10.1016/j.ijheatmasstransfer.2021.121084.
[32] T.R. Goodman, The heat-balance integral—further considerations and refinements, J. Heat Tran. 83 (1) (1961) 83–85, https://doi.org/10.1115/1.3680474.
[33] M.T. Lawder, V. Ramadesigan, B. Suthar, V.R. Subramanian, Extending explicit and linearly implicit ODE solvers for index-1 DAEs, Comput. Chem. Eng. 82 (2015) 283–292, https://doi.org/10.1016/j.compchemeng.2015.07.002.
[34] M.T. Lawder, P.W. Northrop, V.R. Subramanian, Model-based SEI layer growth and capacity fade analysis for EV and PHEV batteries and drive cycles, J. Electrochem. Soc. 161 (14) (2014) A2099, https://doi.org/10.1149/2.1161412jes.
[35] M. Broussely, et al., Main aging mechanisms in Li ion batteries, J. Power Sources 146 (1–2) (2005) 90–96, https://doi.org/10.1016/j.jpowsour.2005.03.172.